Lattice dynamics of the $A15$ compound Nb_3Sb

L. Pintschovius,* H. G. Smith, and N. Wakabayashi†
Solid State Division, Oak Ridge National Laboratory, Oak Ridge, Tennessee 37830

W. Reichardt and W. Weber
Institut für Angewandte Kernphysik I, Kernforschungszentrum Karlsruhe, Postfach 3640, D-7500 Karlsruhe, Federal Republic of Germany

G. W. Webb and Z. Fisk‡
University of California at San Diego, La Jolla, California 92093
(Received 14 March 1983)

The phonon dispersion curves of Nb_3Sb have been studied by inelastic neutron scattering. All the branches have been determined in the main symmetry directions and the results are analyzed with Born—von Kármán models of different complexity. A model with general forces up to the eighth-nearest neighbors gives excellent agreement with experiment. However, a rather good description of the dispersion curves is obtained with a model including axially symmetric forces up to the third-nearest neighbors, which indicates that these interactions are dominant. Temperature effects were found to be very small. Additional experiments were performed on polycrystalline samples to determine directly the phonon density of states. Our results obtained on Nb_3Sb are compared with the available phonon data on Nb_3Sn.

I. INTRODUCTION

Many of the compounds that possess the $A15$ crystal structure exhibit very high superconducting transition temperatures. A knowledge of the lattice dynamics and the detailed phonon behavior of the $A15$ compounds is considered essential in order to obtain a better understanding of their electron-phonon interactions. Inelastic neutron scattering techniques are extremely valuable in this regard, and coupled with complementary techniques, such as ultrasonics, Raman scattering, and superconducting tunneling measurements, they have shed much light on the role of phonons in many superconducting metals, alloys, and compounds.[1]

Obviously, the $A15$ compounds attracting particular interest are those with very high T_c, such as Nb_3Ge, V_3Si, Nb_3Sn, and Nb_3Al. Unfortunately, large single crystals are necessary in order to determine completely the phonon dispersion curves in the search for phonon anomalies. Even larger crystals are needed to measure directly the phonon linewidths. Of the above-mentioned $A15$ compounds, large crystals (>1 cm^3) could be grown only for V_3Si, but the neutron scattering properties are extremely unfavorable for coherent neutron scattering experiments so that only the lowest phonon branches could be determined.[2,3] A similar situation exists for Nb_3Sn where only very small crystals have been grown, but the limited amount of phonon data obtained by inelastic neutron scattering has contributed substantially to furthering the state of knowledge of the electron-phonon interaction in this compound.[3]

It is often very informative to compare the phonon dispersion curves of a moderate- or high-T_c material with a low-T_c or nonsuperconducting material in order to determine which regions, if any, of the dispersion curves are anomalous. This has proved very useful in the past for many different types of superconductors. It applies particularly for the $A15$ compounds, since their phonon dispersion is quite complex and current theories are able to predict changes in the phonon dispersion caused by electron-phonon interactions rather than to predict the phonon dispersion curves in the absence of strong electron-phonon coupling.[4] After we succeeded in growing a large crystal (>1cm^3) of Nb_3Sb ($T_c \simeq 0.2$ K), a material with excellent neutron scattering properties, we performed experiments aiming at a complete determination of the phonon dispersion curves in the main symmetry directions, which may serve as a reference for future results obtained on high-T_c $A15$ compounds.

We should like to mention that Cr_3Si can be seen as a similar reference material with respect to high-T_c compounds, in particular to V_3Si. This compound has been studied recently by Weiss and Rumyantsev[5] and by Jørgensen *et al.*[6] Because of the small neutron scattering cross sections of both Cr and Si, only a limited number of branches could be determined for this compound. Kobbelt *et al.*[7] have measured the phonon density of states of Cr_3Si, which allowed a marked improvement of the model given in Ref. 6.

II. EXPERIMENT

The samples were grown at the University of California at San Diego by chemical vapor deposition. The two largest single crystals had a value of 1.2 and 0.5 cm^3, and both were of excellent quality (mosaic spread of less than 0.2°). Most of the phonon data were obtained on the larger crystal, but for several scans both crystals were mounted

simultaneously, one above the other, in order to give maximum counting rates. The phonon studies were made on the HB-1A, HB-2, and HB-3 triple-axis spectrometers at the Oak Ridge National Laboratory High Flux Isotope Reactor. The final and most complete set of measurements was made on HB-3 with a Be(002) plane as monochromator, and either Be(002) or PG(002) planes as the analyzer in the constant-Q mode of operation with $E'=6$—8 THz. The sample was first oriented with a [110] axis vertical allowing the measurement of all phonon branches in the [001] and [111] directions and most of the phonon branches in the [110] directions. For a determination of some [110] modes with [1$\bar{1}$0] polarization the sample was reoriented to have the [001] axis vertical. In total, some 500 scans have been performed at about 350 points in reciprocal space. Most of the measurements were performed at room temperature, but selected phonons were also investigated at $T=70$ K.

In addition to these experiments, the phonon density of states has been determined on polycrystalline material originating from the same batch as the single crystals. This investigation has been carried out on the TOF1 time-of-flight spectrometer at the FR2 research reactor in Karlsruhe at room temperature.

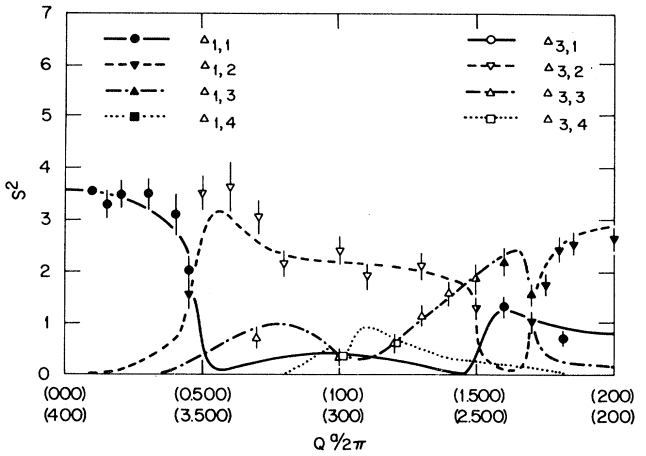

FIG. 1. Comparison of calculated and observed inelastic structure factors along [ζ00]. Branches not included in the figure have zero structure factors. Experimental points are normalized to the intensity of the $\Delta_{1,1}$ branch at $Q=0.100$, where the calculated structure factor depends only very little on the model.

III. RESULTS AND ANALYSIS

A. Identification of the experimental phonon groups

Although the $A15$ structure is cubic, its lattice dynamics is rather complex, with two A_3B units in the primitive cell which gives $3n=24$ branches in the Brillouin zone. Although, because of degeneracies, this number is reduced to 17 and 16 in the [001] and [111] directions, respectively, it is extremely difficult, if not impossible, to identify all the branches without a group-theoretical study and a knowledge of the polarization vectors of the modes. For the latter, it is necessary to have a lattice-dynamical model to calculate the expected intensities of the phonon groups.

A group-theoretical analysis for all the symmetry points and directions of the $A15$ structure has been published by Achar and Barsch,[8] and these results have proved useful in the initial stages of this work. Later, we became aware that the symmetry properties of the $A15$ structure had earlier been investigated by other authors.[9,10] Since their notation is commonly used in the literature when dealing with the electronic properties of these compounds, we adopt it also for the following.

The calculated results reported here are based on Born—von Kármán force-constant models described below. An initial set of force constants was deduced from a limited amount of experimental data. Only phonon groups from branches that were thought to be reliably identified were used. The initial force constants were then used to calculate the frequencies, polarization vectors, and intensities of all the branches in the [001], [111], and [110] directions. These results were used to identify additional phonon groups as well as to indicate where in reciprocal space previously unobserved groups should be measured. The additional information was used to refine the model, and after a few iterations all the modes of the Γ, X, and R points were confidently assigned. Most of the modes at the M point and in the Δ, Σ, and Λ directions could also be assigned with reasonable confidence. As an example, the calculated and observed inelastic structure factors, plotted in Fig. 1 for momentum transfers $\vec{Q}$ along the [100] direction, demonstrate the dependability of the model. Since, for all values of q, scans have been performed at many points in reciprocal space, the assignment could often be based on redundant information.

For some values of $\vec{q}$ there is a great deal of mixing of the polarization vectors of certain branches. Where there is appreciable overlap of the experimental dispersion curves because of the instrumental resolution, the assignment is less certain. However, in these cases the resulting uncertainty is not too serious, because all the branches in question have similar frequencies at these $\vec{q}$ values, and therefore it is felt that errors of that kind would have a minimal effect on the force constants. Our results are summarized in Fig. 2 and Table I.

B. Lattice-dynamical models

The simplest way of analyzing the experimental data is to use a Born—von Kármán model based on axially symmetric forces between, e.g., atoms (l,κ) and (l',κ'), where l,l' denote lattice sites and κ,κ' label the atoms in the unit cell. The force-constant matrix between these atoms then has the form

$$\phi(l,\kappa\alpha;l'\kappa',\beta)=-F(l\kappa;l',\kappa')\hat{r}_\alpha(l,\kappa;l',\kappa')\times\hat{r}_\beta(l,\kappa;l',\kappa')-G(l,\kappa;l',\kappa')\times[\delta_{\alpha\beta}-\hat{r}_\alpha(l,\kappa;l',\kappa')\hat{r}_\beta(l,\kappa;l'\kappa')]\ .$$

Here $\vec{r}(l,\kappa;l',\kappa')=\vec{R}(l,\kappa)-\vec{R}(l',\kappa')$ is the distance vector between the atoms (l,κ) and (l',κ'), and $\hat{r}$ indicates a vector

TABLE I. Nb_3Sb phonon frequencies (THz) at room temperature. Symmetry classifications are given on top of each column. If there are several modes for a certain q value having the same symmetry, the highest frequency is printed below the symmetry symbol, the next highest in the column to the right, etc. Numbers printed in the middle of two columns denote the average of the frequencies of two modes, which could not be resolved.

			Γ		
Γ_{12}	Γ_2	$\Gamma_{25'}$	$\Gamma_{15'}$	Γ_{25}	Γ_{15}
7.6±0.1	7.3±0.1	5.0±0.1	4.78±0.05	6.5±0.08;3.45±0.05	5.72±0.08;4.45±0.05
			X		
X_1		X_2	X_3	X_4	
7.85±0.1;6.4±0.08;4.92±0.05;4.45±0.1		4.91±0.05	6.25±0.1;4.3±0.1;2.48±0.05	6.35±0.15;5.56±0.08;5.05±0.15;2.48±0.05	
			M		
M_1	M_2		M_3	M_5	M_6
6.3±0.15;...	8.0±0.1;5.55±0.15;4.3±0.1		5.48±0.05	...;6.55±0.1	...;6.25±0.1
M_7	M_8		M_9		M_{10}
4.45±0.1	4.07±0.05		6.55±0.1;5.2±0.1;4.5±0.08		6.51±0.06;5.15±0.1;2.75±0.05
			R		
$R_{1,2}$			R_3		R_4
4.76±0.05			5.40±0.06		6.8±0.08;5.47±0.06;4.23±0.07
			Δ		
	Δ_1		$\Delta_{1'}$	Δ_2	$\Delta_{2'}$
0.1	...;...;...;1.12±0.03		4.88±0.1	...;...;6.4±0.08;3.47±0.07	...
0.15	7.6±0.08;5.72±0.06;4.6±0.05;1.7±0.03		...	...;...;...;3.5±0.05	...
0.2	7.45±0.15;...;4.82±0.05;2.3±0.05		4.65±0.1	...;7.25±0.1;6.2±0.07;3.6±0.1	4.95±0.1
0.25	7.63±0.08;5.55±0.08;4.9±0.1;...		...	...;...;...;3.8±0.1	...
0.3	...;5.65±0.1;5.36±0.1;3.25±0.03		4.9±0.15	7.72±0.08;7.12±0.1;5.98±0.06;...	5.06±0.03
0.35	...;...;5.28±0.07;...		...	7.64±0.08;...;...;...	...
0.4	7.75±0.1;5.95±0.1;5.15±0.07;4.1±0.05		4.85±0.1	...;6.93±0.08;5.5±0.06;4.52±0.08	4.93±0.1
0.45	...;...;4.98±0.1;4.5±0.1		...	...;...;...;...	...
			Δ_5		
0.1	...;...;5.25±0.08;4.87±0.05;4.25±0.1;3.36±0.05;0.55±0.03;				
0.15	...;...;...;5.02±0.05;...;...;...;				
0.2	6.52±0.08;5.95±0.05;5.2±0.08;5.02±0.08;4.35±0.07;3.25±0.05;1.1±0.03;				
0.25	...;6.04±0.01;5.17±0.06;4.28±0.1;...;...;				
0.3	6.55±0.08;...;5.35±0.06;4.95±0.08;4.4±0.1;3.0±0.05;1.62±0.03;				
0.4	6.5±0.1;6.22±0.07;5.5±0.01;5.2±0.2;4.35±0.1;2.78±0.04;2.06±0.03;				

TABLE I. (*Continued.*)

	Σ	
	Σ_1	Σ_2
0.1	. . .;. . .;. . .;4.98±0.07;4.44±0.06;. . .;1.51±0.02;	. . .;4.95±0.05;. . .;. . .
0.15	7.52±0.1;6.4±0.07;. . .;. . .;. . .;. . .;2.2±0.03;	. . .;5.16±0.1;. . .;. .
0.2	7.35±0.1;. . .;. . .;5.09±0.08;4.65±0.2;3.5±0.1;2.92±0.04;	6.54±0.06;5.35±0.15;5.15±0.15;3.1±0.1
0.25	. . .;6.25±0.15;5.8±0.15;. . .;. . .;3.7±0.1;3.3±0.05;	. . .;. . .;. . .;. . .;
0.3	7.36±0.1;6.4±0.2;5.9±0.1;5.1±0.1;5.0±0.1;4.0±0.1;3.9±0.1;	6.6±0.07;5.3±0.1;5.2±0.1;2.9±0.1
0.35	. . .;. . .;. . .;5.14±0.07;4.98±0.05;4.15±0.08;. . .;	. . .;. . .;. . .;. . .;
0.4	7.05±0.1;6.15±0.1;5.8±0.15;5.28±0.1;4.9±0.1;4.45±0.07;4.3±0.08;	6.58±0.07;5.45±0.1;5.15±0.08;. . .
0.45	. . .;. . .;. . .;5.16±0.1;. . .;. . .;. . .;	

	Σ_3	Σ_4
0.1	. . .;. . .;4.85±0.1;4.35±0.06;0.8±0.02;	. . .;. . .;. . .;. . .;5.0±0.1;4.53±0.08;. . .;0.97±0.03;
0.15	5.92±0.06;. . .;. . .;4.24±0.05;1.17±0.02;	7.8±0.1;7.3±0.1;6.3±0.1;5.6±0.1;. . .;4.68±0.06;. . .;. . .;
0.2	. . .;. . .;4.9±0.1;4.16±0.05;1.53±0.02	. . .;7.26±0.15;6.25±0.1;5.7±0.1;5.25±0.1;4.83±0.1;. . .;1.97±0.04;
0.25	6.12±0.1;. . .;4.92±0.06;4.1±0.05;1.82±0.02;	. . .;7.22±0.1;6.14±0.1;5.5±0.15;. . .;. . .;. . .;. . .;
0.3	6.4±0.2;5.3±0.15;4.7±0.07;4.06±0.05;2.16±0.02;	7.9±0.1;7.02±0.07;5.9±0.1;5.6±0.1;5.4±0.08;5.2±0.1;3.9±0.1;2.83±0.03;
0.35	. . .;. . .;4.58±0.05;3.96±0.05;2.43±0.03;	7.8±0.08;6.7±0.15;6.13±0.15;5.6±0.1;5.3±0.1;4.98±0.05;4.15±0.05;3.65±0.03;
0.4	6.56±0.06;5.07±0.07;4.5±0.1;4.15±0.05;2.58±0.04;	. . .;. . .;. . .;. . .;. . .;. . .;4.4±0.13;4.02±0.05;

	Λ		
	Λ_1	Λ_2	Λ_3
0.1	5.85±0.08;. . .;4.45±0.05;1.78±0.04	7.15±0.2;. . .;5.1±0.1;. . .;	7.6±0.2;6.4±0.1;. . .;5.1±0.1;4.90±0.08;4.48±0.05;3.36±0.05;1.1±0.03;
0.15	. . .;5.06±0.1;4.38±0.05;2.52±0.1	. . .;. . .;. . .;. . .;	. . .;. . .;5.72±0.08;. . .;. . .;. . .;. . .;. . .;
0.2	5.8±0.15;. . .;4.52±0.05;3.25±0.04	7.28±0.1;6.3±0.1;5.45±0.1;3.60±0.05;	7.45±0.1;6.38±0.1;. . .;5.3±0.15;5.0±0.15;4.75±0.12;3.50±0.05;2.18±0.04;
0.25	. . .;5.3±0.15;4.73±0.05;3.65±0.05	7.2±0.1;5.9±0.1;. . .;. . .;	. . .;. . .;5.64±0.1;5.25±0.1;5.0±0.15;4.8±0.1;3.62±0.05;. . .;
0.3	. . .;5.4±0.1;5.0±0.06;3.83±0.07	7.25±0.1;5.9±0.1;5.4±0.1;3.88±0.05;	. . .;6.25±0.05;5.75±0.1;5.4±0.15;5.1±0.1;3.68±0.05;3.08±0.05;
0.35	. . .;5.5±0.15;5.15±0.1;. . .;	. . .;. . .;. . .;. . .;	. . .;. . .;5.55±0.15;5.0±0.15;. . .;. . .;
0.4	6.25±0.15;5.5±0.1;5.1±0.1;4.06±0.05	7.1±0.15;5.88±0.08;5.35±0.1;4.1±0.1;	7.2±0.1;6.45±0.1;5.55±0.08;5.3±0.1;5.05±0.1;4.95±0.1;. . .;3.85±0.05;

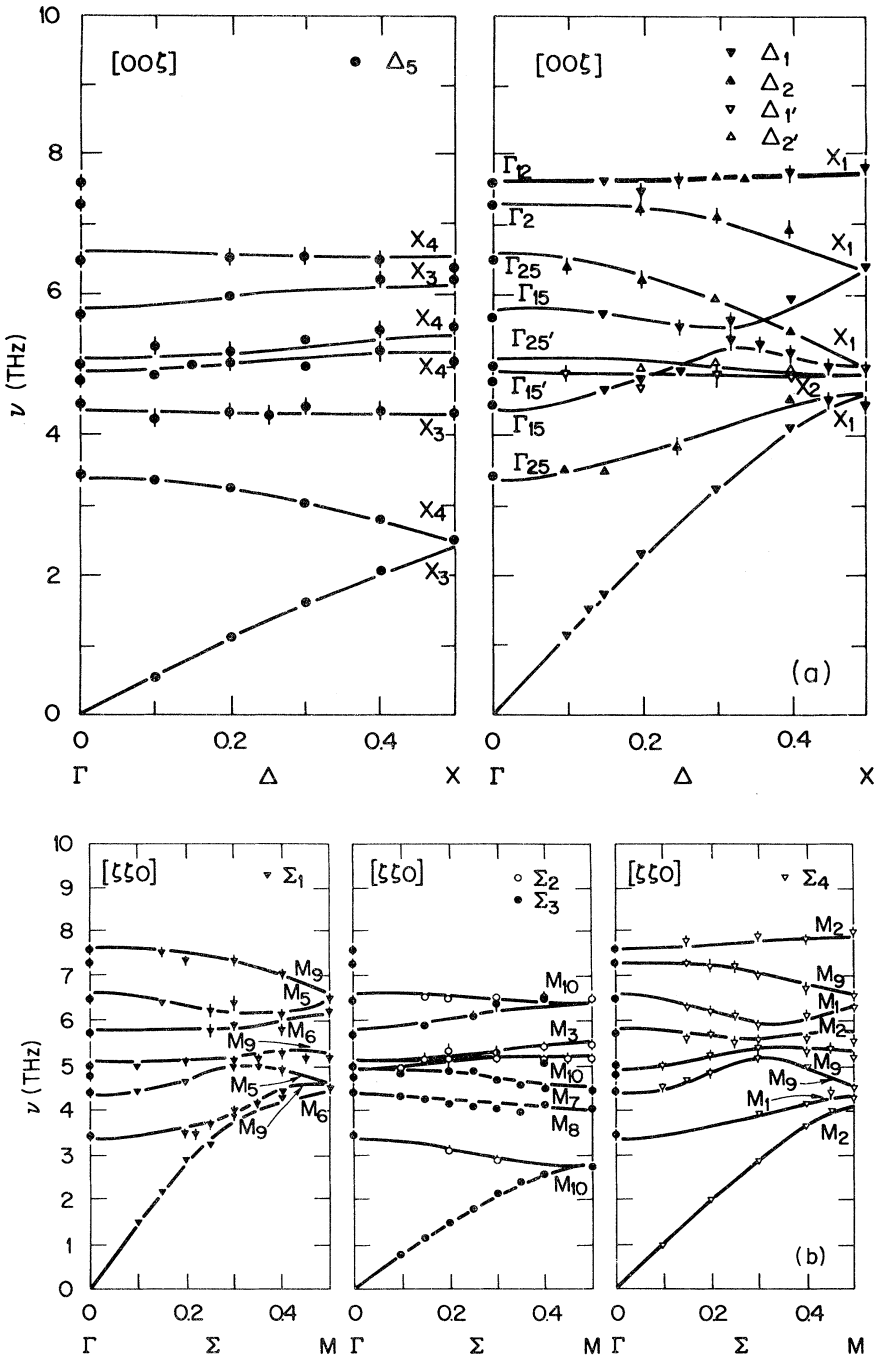

FIG. 2. Phonon dispersion curves of Nb_3Sb in the main symmetry directions at room temperature. (a) [00ζ] direction, (b) [ζζ0] direction, and (c) [ζζζ] direction. Lines are the result of a fit based on an eighth-NN Born—von Kármán model.

of unit length. F and G are the "longitudinal" and "transverse" force constants, respectively. They are assumed to be equal for all pairs of atoms having the same distance and the same sublattice specifications. Thus the force-constant matrix ϕ has the two linearly independent matrix elements and is symmetric in the Cartesian indices α and β.

In general, however, ϕ may have more than two independent matrix elements. Their maximum number is determined by the symmetry of the crystal and may be nine in the case of lowest symmetry. Group-theoretical techniques allow one to find the maximum number of independent elements in ϕ; these techniques are described, e.g., in Ref. 11.

We have set up a computer program which allows the use of either axially symmetric or general force constants

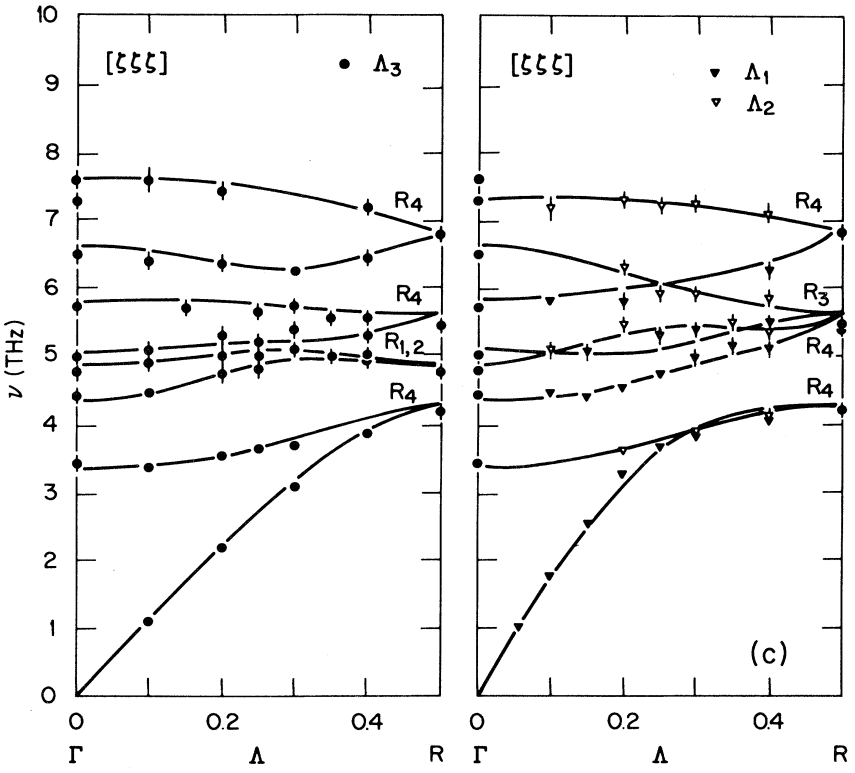

FIG. 2. (*Continued.*)

for any pair of atoms. In practice, we have investigated only models where the force constants do not extend beyond the distance of the first primitive lattice vector. In Table II, these force-constant matrices are listed both for axially symmetric and general forces. There are eight different neighbor pairs within the distance of a lattice constant. We note that the general forces for first-nearest neighbors (NN) (*A*-atom intrachain coupling) exhibit two different transverse force constants. These are interchanged when going in the opposite direction along the chain. Furthermore, there are two different kinds of seventh-NN pairs. One consists of *A* atoms situated at two adjacent parallel chains, the other is made up by two *A* atoms of the same chain.

We have fitted the models to 283 experimental phonon frequencies measured at the symmetry points Γ, *X*, *M*, and *R*, and 23 additional points along the symmetry lines Δ, Σ, and Λ of the Brillouin zone. When calculating the root-mean-square (rms) deviations, we have incorporated a weight factor proportional to $1/\omega_{\rm ph}$ to account for the larger experimental errors at higher frequencies.

In Table III we present various models of increasing complexity. The models I—III are restricted to axially symmetric forces, while model IV employs general forces. In the models I and II, the force constants (FC's) are limited to within the third-NN distance, i.e., including only the FC's of the first intrachain, interchain, and *A*-*B* pairs. The longitudinal FC's of these three pairs represent the dominant forces in the Nb_3Sb crystal. When we incorporate the transverse FC's, especially for the interchain pair, we find a considerable decrease of the rms value. Thus, model II with only six parameters already gives a satisfactory agreement with experiment. Further improvement is achieved by including more distant neighbors. Here the most important additional FC's are the longitudinal FC's of the second-NN *A*-*B* and fourth-NN *A*-*A* interactions [denoted by $(B\text{-}A)^{\rm II}$ and $(A\text{-}A)^{\rm IV}$ in Table III]. In model IV, general forces have been assumed for all neighbor pairs (we have omitted the sixth-NN forces, as they turned out to be very small). Its 31 FC's are listed in Table IV. The excellent agreement with experiment is obvious from Fig. 2.

We note that in all the models investigated the values of the near-FC's are rather stable. Since the closest Nb-Nb distance in Nb_3Sb is about 10% shorter than in bcc Nb, one would expect the first-NN longitudinal FC to be the dominant one in this compound. Indeed, this FC is the largest one, and consequently the highest modes observed at Γ are the Γ_{12} and Γ_2 modes which correspond to out-of-phase near-neighbor motions along the chains (see Fig. 3). However, the second-NN and even the third-NN FC's are not much smaller than the first-NN FC's, which implies that with respect to the lattice dynamics, Nb_3Sb cannot be regarded as a linear-chain compound.

Since model II, which includes interactions up to the third-NN's only, already gives a satisfactory description of the experimental frequencies, interactions between more distant neighbors seem to be of minor importance. This is not astonishing in view of the fact that Nb_3Sb is a very-low-T_c superconductor: Whereas all good superconduc-

TABLE II. FC matrices for pairs 1–8 for both axially symmetric and general forces. In the general case, pair 1 has two different transverse FC's β and γ which interchange when the distance vector is changed. Pair 7 has two different matrices depending on whether interchain atoms (t) or intrachain atoms (l) are coupled.

No. of NN pairs	Specification	Distance vector	Positions of atoms (1)	(2)	Force-constant matrix $\phi_{\kappa\beta}$ Axially symmetric	General Symmetric	General Antisymmetric	Number of independent matrix elements	Distance in units of α
		0.5	0.25	−0.25	$\begin{pmatrix} F & 0 & 0 \\ 0 & G & 0 \\ 0 & 0 & G \end{pmatrix}$	$\begin{pmatrix} \alpha & 0 & 0 \\ 0 & \beta & 0 \\ 0 & 0 & \gamma \end{pmatrix}$	$\begin{pmatrix} 0 & 0 & 0 \\ 0 & 0 & 0 \\ 0 & 0 & 0 \end{pmatrix}$		
1	$(A\text{-}A)^{\mathrm{I}}$	0	0	0				3	0.500
		0	0.5	0.5					
		−0.5	0.25	0.75	$\begin{pmatrix} F & 0 & 0 \\ 0 & G & 0 \\ 0 & 0 & G \end{pmatrix}$	$\begin{pmatrix} \alpha & 0 & 0 \\ 0 & \gamma & 0 \\ 0 & 0 & \beta \end{pmatrix}$	$\begin{pmatrix} 0 & 0 & 0 \\ 0 & 0 & 0 \\ 0 & 0 & 0 \end{pmatrix}$		
1	$(A\text{-}A)^{\mathrm{I}}$	0	0	0				3	0.500
		0	0.5	0.5					
		0.5	0	0.5	$\frac{1}{5}\begin{pmatrix} 4F+G & 2F-2G & 0 \\ 2F-2G & F+4G & 0 \\ 0 & 0 & 5G \end{pmatrix}$	$\begin{pmatrix} \alpha & \delta & 0 \\ \delta & \beta & 0 \\ 0 & 0 & \gamma \end{pmatrix}$	$\begin{pmatrix} 0 & \epsilon & 0 \\ \bar{\epsilon} & 0 & 0 \\ 0 & 0 & 0 \end{pmatrix}$		
2	$(B\text{-}A)^{\mathrm{I}}$	0.25	0	0.25				5	0.559
		0	0	0					
		0.5	0.5	0	$\frac{1}{6}\begin{pmatrix} 4F+2G & 2F-2G & 2F-2G \\ 2F-2G & F+5G & F-G \\ 2F-2G & F-G & F+5G \end{pmatrix}$	$\begin{pmatrix} \alpha & \delta & \delta \\ \delta & \beta & \gamma \\ \delta & \gamma & \beta \end{pmatrix}$	$\begin{pmatrix} 0 & \mu & \bar{\mu} \\ \bar{\mu} & 0 & \epsilon \\ \mu & \bar{\epsilon} & 0 \end{pmatrix}$		
3	$(A\text{-}A)^{\mathrm{II}}$	0.25	−0.25	−0.5				6	0.612
		0.25	0	−0.25					
		0.5	0	0.5	$\frac{1}{3}\begin{pmatrix} F+2G & F-G & F-G \\ F-G & F+2G & F-G \\ F-G & F-G & F+2G \end{pmatrix}$	$\begin{pmatrix} \alpha & \beta & \beta \\ \beta & \alpha & \beta \\ \beta & \beta & \alpha \end{pmatrix}$	$\begin{pmatrix} 0 & \gamma & \bar{\gamma} \\ \bar{\gamma} & 0 & \gamma \\ \gamma & \bar{\gamma} & 0 \end{pmatrix}$		
4	$(B\text{-}B)^{\mathrm{I}}$	0.5	0	0.5				3	0.866
		0.5	0	0.5					
		0.75	0	0.75	$\frac{1}{13}\begin{pmatrix} 9F+4G & 6F-6G & 0 \\ 6F-6G & 4F+9G & 0 \\ 6F-6G & 0 & 13G \end{pmatrix}$	$\begin{pmatrix} \alpha & \delta & 0 \\ \delta & \beta & 0 \\ 0 & 0 & \gamma \end{pmatrix}$	$\begin{pmatrix} 0 & \epsilon & 0 \\ \bar{\epsilon} & 0 & 0 \\ 0 & 0 & 0 \end{pmatrix}$		
5	$(B\text{-}A)^{\mathrm{II}}$	0.5	0	0.5				5	0.901
		0	0	0					
		0.75	0	0.75	$\frac{1}{14}\begin{pmatrix} 9F+5G & 6F-6G & 3F-3G \\ 6F-6G & 4F+10G & 2F-2G \\ 3F-3G & 2F-2G & F+13G \end{pmatrix}$	$\begin{pmatrix} \alpha & \epsilon & \mu \\ \epsilon & \beta & \delta \\ \mu & \delta & \gamma \end{pmatrix}$	$\begin{pmatrix} 0 & \lambda & \bar{\kappa} \\ \bar{\lambda} & 0 & \nu \\ \kappa & \bar{\nu} & 0 \end{pmatrix}$		
6	$(A\text{-}A)^{\mathrm{III}}$	0.50	0.5	0				9	0.935
		0.25	−0.25	−0.50					
		1.0	0.5	−0.5	$\begin{pmatrix} F_t & 0 & 0 \\ 0 & G_t & 0 \\ 0 & 0 & G_t \end{pmatrix}$	$\begin{pmatrix} \alpha_t & 0 & 0 \\ 0 & \beta_t & 0 \\ 0 & 0 & \gamma_t \end{pmatrix}$	$\begin{pmatrix} 0 & \delta_t & 0 \\ \delta_t & 0 & 0 \\ 0 & 0 & 0 \end{pmatrix}$		
7	$(A\text{-}A)_t^{\mathrm{IV}}$	0	0.25	0.25				4	1.000
		0	0	0					
		1.0	0.25	−0.75	$\begin{pmatrix} F_l & 0 & 0 \\ 0 & G_l & 0 \\ 0 & 0 & G_l \end{pmatrix}$	$\begin{pmatrix} \alpha_l & 0 & 0 \\ 0 & \beta_l & 0 \\ 0 & 0 & \beta_l \end{pmatrix}$	$\begin{pmatrix} 0 & 0 & 0 \\ 0 & 0 & 0 \\ 0 & 0 & 0 \end{pmatrix}$		
7	$(A\text{-}A)_l^{\mathrm{IV}}$	0	0	0				2	1.000
		0	0.5	0.5					
		1.0	0	−1.0	$\begin{pmatrix} F & 0 & 0 \\ 0 & G & 0 \\ 0 & 0 & G \end{pmatrix}$	$\begin{pmatrix} \alpha & 0 & 0 \\ 0 & \beta & 0 \\ 0 & 0 & \gamma \end{pmatrix}$	$\begin{pmatrix} 0 & 0 & 0 \\ 0 & 0 & 0 \\ 0 & 0 & 0 \end{pmatrix}$		
8	$(B\text{-}B)^{\mathrm{II}}$	0	0	0				3	1.000
		0	0	0					

TABLE III. FC's for models I—III. F denotes longitudinal and G transverse FC's. For comparison, some FC's of model IV are also given.

No. of NN pairs	Specification	Distance	Force constants (10^3 dyn/cm) I F	I G	II F	II G	III F	III G	IV
1	$(A\text{-}A)^{I}$	0.500	57.1		65.1	2.2	64.1	4.6	$64.4^{-3.7}_{+16.2}$
2	$(B\text{-}A)^{I}$	0.559	48.2		46.8	0.26	45.5	0.5	5 parameter
3	$(A\text{-}A)^{II}$	0.612	24.7		15.4	5.4	13.5	2.6	6 parameter
4	$(B\text{-}B)^{I}$	0.866					−0.9	0.8	3 parameter
5	$(B\text{-}A)^{II}$	0.901					3.4	−1.9	5 parameter
6	$(A\text{-}A)^{III}$	0.935					1.2	0.4	
7_t	$(A\text{-}A)_t^{IV}$	1.000					4.7	0.4	4 parameter
7_l	$(A\text{-}A)_l^{IV}$	1.000					4.7	0.4	5.8 1.0
8	$(B\text{-}B)^{II}$	1.000					3.1	−0.1	$8.5^{-0.3}_{+0.0}$
			No. of parameters						
			3		6		16		31
			rms value						
			0.313	0.169		0.116			0.088

tors so far investigated exhibit pronounced anomalies in their phonon dispersion curves,[1] low- or zero-T_c materials generally have rather "normal" dispersion curves, which can be fairly well described by models including short-range forces only. In Nb_3Sb long-range forces are small, but not negligible because of the following two reasons.

(i) The major improvement when going from model II to models III and IV is achieved by including forces which couple atoms with the same sublattice label, thereby allowing the trace of the dynamical matrix to vary with q. Using e.g., model III, we find the trace at Γ point to be 4.23×10^6 dyn/cm; at point X, 4.37×10^6; at point M, 4.51×10^6; and at point R, 4.65×10^6, which is in close agreement to the trends observed in the experimental data. The 10% increase of the average force constant between Γ and R may be related to changes in the electronic screening.

(ii) Although model II describes most of the branches quite satisfactorily, it exhibits clear deficiencies in describing the branches starting from the $\Gamma_{25'}$ and $\Gamma_{15'}$ modes, e.g., in the [100] direction, the increase in frequency of the corresponding Δ_5 branches when going to the zone boundary cannot be reproduced by this model. It is probably not accidental that deficiencies of a short-range FC model show up just at this point. In the moderate to high-T_c compounds, $Nb_{3.2}Ge_{0.8}$,[12,13] $Nb_{3.1}Ga_{0.9}$,[13,14] and Nb_3Sn,[12,15] the $\Gamma_{25'}$ and $\Gamma_{15'}$ modes are strongly depressed compared to Nb_3Sb. It looks as if there is a reminiscence of this anomaly also in Nb_3Sb. The $\Delta_{1'}$, and $\Delta_{2'}$ branches, which involve motions very similar to the $\Gamma_{15'}$ and $\Gamma_{25'}$ modes, i.e., a buckling of the chains, are very flat throughout the Brillouin zone. The corresponding Δ_5 branches increase in frequency in accordance to the change in the vibrational pattern which involves more and more Sb motion on going toward the zone boundary.

C. Phonon density of states

Inelastic neutron scattering experiments on polycrystalline samples yield a generalized phonon density of states $G(\nu)$, which is a weighted average of the partial density of states $F_i(\nu)$ of all atoms in the unit cell,

$$G(\nu)=\sum_i \frac{\sigma_i}{M_i}F_i(\nu)\Big/\sum_i \frac{\sigma_i}{M_i}\ .$$

Here σ_i are the neutron scattering cross sections and M_i

TABLE IV. FC's of model IV (general forces).

No. of NN pairs	Specification	Force constants (10^3 dyn/cm) α	β	γ	δ	ϵ	μ
1	$(A\text{-}A)^{I}$	64.4	−3.7	16.2			
2	$(B\text{-}A)^{I}$	36.4	6.0	−1.2	8.3	−7.0	
3	$(A\text{-}A)^{II}$	7.4	6.5	2.0	7.0	−0.4	4.1
4	$(B\text{-}B)^{I}$	3.6	0.9	−0.4			
5	$(B\text{-}A)^{II}$	2.9	1.5	−0.8	4.6	−3.8	
6	$(A\text{-}A)^{III}$						
7_t	$(A\text{-}A)_t^{IV}$	10.3	1.2	−2.2	−2.1		
7_l	$(A\text{-}A)_l^{IV}$	5.8	1.0				
8	$(B\text{-}B)^{II}$	−8.5	−0.3	−0.0			

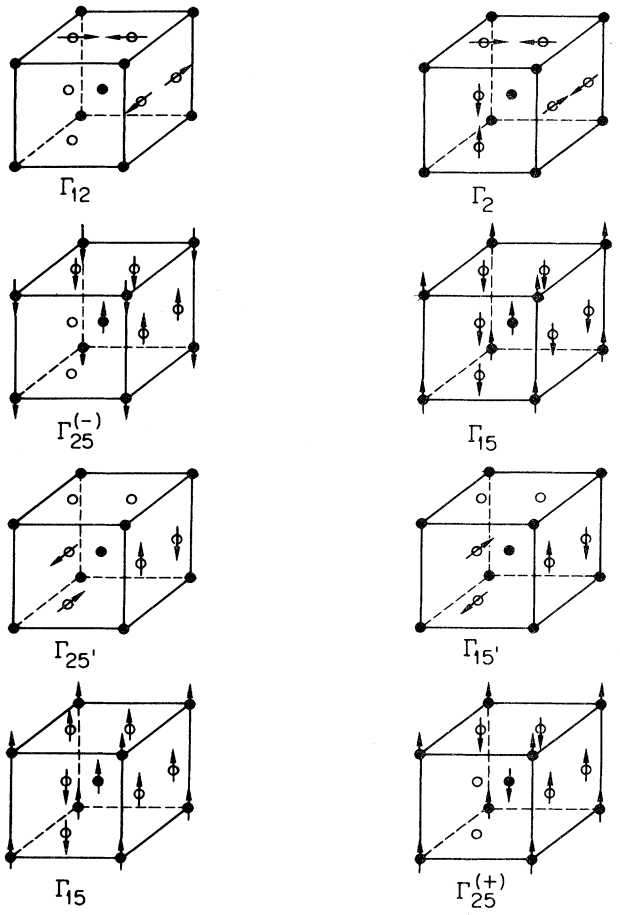

FIG. 3. Pattern of motion for the optic modes at the Γ point in $A15$ compounds.

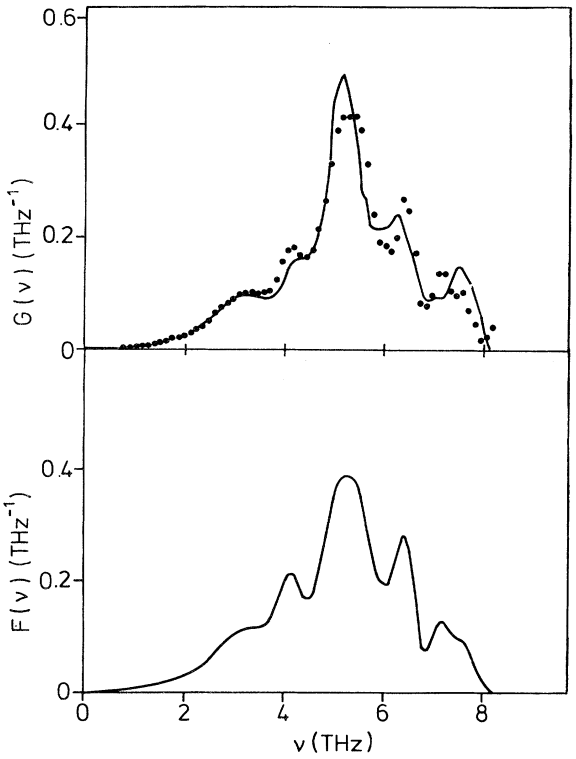

FIG. 4. Phonon density of states in Nb_3Sb. Upper half of the figure shows a comparison of the calculated and experimentally determined generalized density of states

$$G(\nu)=\sum_i \frac{\sigma_i}{M_i}F_i(\nu)\Big/\sum_i \frac{\sigma_i}{M_i},$$

where σ_i denotes the neutron cross section, M_i denotes the atomic mass, and $F_i(\nu)$ denotes the partial density of states of the different atoms in the unit cell. Lower half of the figure shows the density of states $F(\nu)$, which is derived from the experimentally determined $G(\nu)$ by calculating the correction factor $F(\nu)/G(\nu)$ using the Born—von Kármán model described in the text.

are the masses of the atoms. For a direct comparison with experiment, $G(\nu)$ was calculated using model IV and then broadened by the experimental resolution. As can be seen from Fig. 4, the agreement between model and experiment is quite satisfactory. The small differences are presumably due only to deficiencies of the model, but significant contributions may come from experimental errors in the phonon data ($\Delta\nu/\nu\approx\pm 0.1$ THz). In order to evaluate the true phonon density of states $F(\nu)$, the experimentally determined generalized density of states was multiplied by a correction factor $E(\nu)/G(\nu)$ calculated with the aid of model IV (see the lower half of Fig. 4). Since this model yields an excellent description of the data, and since the correction factor is not very dependent on the model parameters, we think the resultant $F(\nu)$ to be quite accurate.

D. Low-temperature results

There is no evidence from other experiments, such as temperature-dependence resistivity studies, to suggest any kind of phase transition, real or incipient. This is in full agreement with the results of our low-temperature investigations: The observed frequency changes between room temperature and 70 K are very small ($|\Delta\nu/\nu| \lesssim 3\%$) and mostly positive. The only exception was found for the TA[110] modes with polarization [1$\bar{1}$0], where a slight frequency decrease upon cooling was observed for $q<0.3q_{\max}$.

Two modes in Nb_3Sb have been observed by Raman scattering techniques, i.e., the Γ_{12} and the $\Gamma_{25'}$ modes.[15] The values of the optically determined frequencies and their temperature dependence are in excellent agreement with our neutron scattering results.

E. Comparison with data for Nb_3Sn

As mentioned in the Introduction, Nb_3Sb was investigated as a reference compound, and therefore we want to compare the limited phonon dispersion curves of Nb_3Sn obtained by inelastic neutron scattering[3] with the results of this study. Since the atomic masses involved are almost identical, the observed differences can be attributed directly to differences in their electronic properties. The

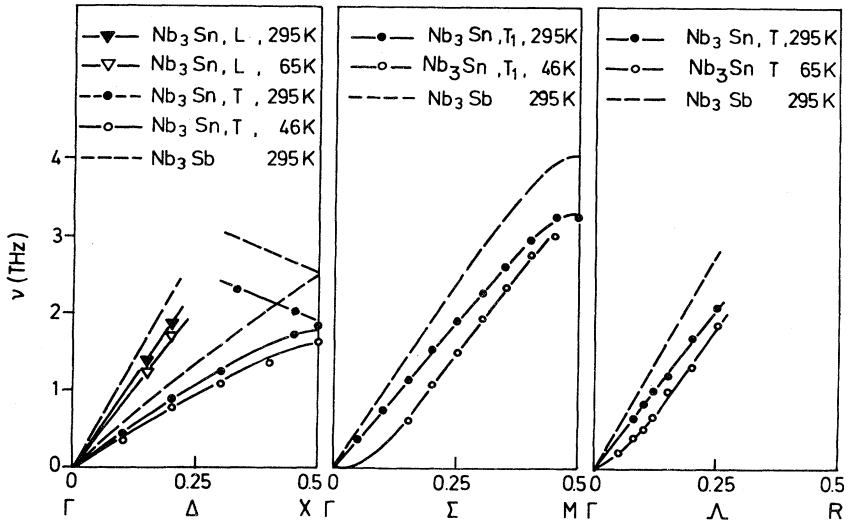

FIG. 5. Comparison of low-frequency phonons in Nb_3Sb and Nb_3Sn. Nb_3Sn data are taken from Ref. 3. For Nb_3Sb only the room-temperature data are plotted. Low-temperature data do not deviate from the room-temperature data by more than 3%.

electron-phonon coupling λ is much larger in Nb_3Sn ($\lambda=1.4$) than in Nb_3Sb ($\lambda=0.4$) reflecting the large differences in their superconducting transition temperatures. Consequently, it is not astonishing that an appreciable overall softening of the acoustic modes in Nb_3Sn compared to Nb_3Sb is found all the way out to the zone boundary (see Fig. 5). Furthermore, a pronounced softening of these modes is observed in Nb_3Sn upon cooling, especially for the TA[110] with polarization [1$\bar{1}$0], reflecting the instability of the A15 lattice in this high-T_c superconductor (Nb_3Sn undergoes a cubic-to-tetragonal phase transformation around 45 K).

In Fig. 6 the density of states (DOS) of Nb_3Sb is compared to that of Nb_3Sn.[16] Again, a considerable softening of the phonon frequencies in Nb_3Sn is visible which extends to the upper end of the spectrum. Finally, a comparison of the Γ_{12} and $\Gamma_{25'}$ modes, which in both compounds could be determined by Raman scattering,[15,17] shows a drastic reduction of the frequencies when going from Nb_3Sb to Nb_3Sn. The frequency decrease amounts to 24% and 20%, respectively, at room temperature and as much as 43% for the Γ_{12} mode at 80 K.

Taking all the available information together, we set up a simple Born–von Kármán model for the lattice dynamics of Nb_3Sn. Although this model is certainly too crude to describe the details of the phonon dispersion curves of Nb_3Sn, we believe that the basic features of our analysis are correct. As can be seen from Fig. 7, the calculated phonon DOS compares fairly well with the experimental values. On the basis of this model it turns out that the differences between the phonon spectra of Nb_3Sn and Nb_3Sb are not just a simple scaling (on the average $\Delta\nu/\nu\approx 12\%$), but some modes are much more affected

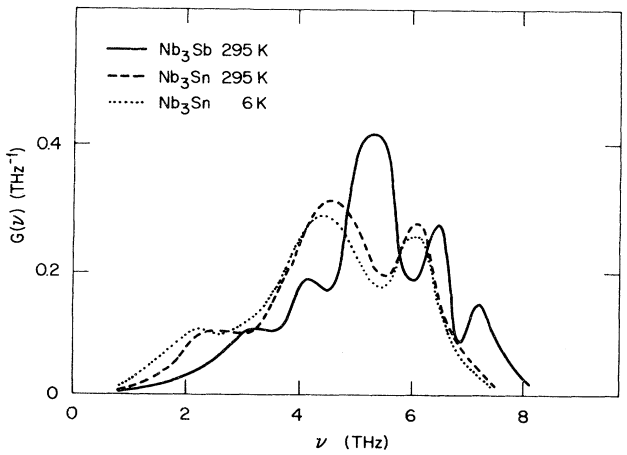

FIG. 6. Comparison of the phonon density of states in Nb_3Sn (after Ref. 16) and Nb_3Sb. For Nb_3Sb the phonon density of states has been measured only at room temperature. From the low-temperature phonon measurements we conclude that there is a slight hardening of the phonon spectrum when going from 295 to 70 K (on the average $\Delta\nu/\nu\approx 1.5\%$).

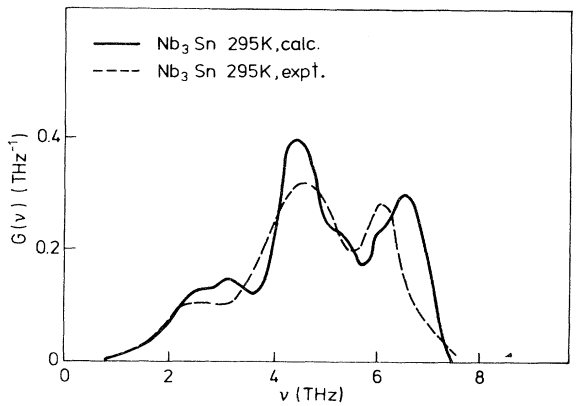

FIG. 7. Comparison of the calculated and experimentally determined generalized density of states for Nb_3Sn at room temperature. Experimental data are taken from Ref. 16.

than others, e.g., at the Γ point the frequency decrease is strongest for the Γ_{12} and Γ_2 modes and the velocities of sound, whereas for the other modes the effect is considerably smaller or even of opposite sign. (Comparing frequencies of the Γ_{15} and Γ_{25} modes one has, of course, to bear in mind that the eigenvectors may be somewhat different in the two compounds.) The differences in the phonon frequencies can be traced back to differences in the FC's: It appears that the most pronounced change occurs for the NN Nb-Nb longitudinal FC, which is reduced almost by a factor of 2, whereas on the other hand the Nb-Nb interchain coupling remains about the same.

IV. CONCLUDING REMARKS

The main objective of our investigation was to provide information about the "normal" phonon dispersion curves of an $A15$ compound, i.e., dispersion curves in the absence of strong electron-phonon coupling effects. As anticipated from the very low T_c of Nb_3Sb, our results show that the lattice dynamics of this compound is indeed largely dominated by short-range forces. It is true that a careful analysis reveals that long-range forces, and hence electron-phonon coupling effects are not negligible in this material; however, these effects are not so large as to prevent the use of Nb_3Sb as a reference compound for comparisons with high-T_c $A15'$ compounds. A comparison of our data with the limited data available for Nb_3Sn shows drastic differences between the lattice dynamics of the two compounds. As in other classes of compounds containing high-T_c superconductors, the phonon dispersion curves of $A15$ compounds apparently contain detailed information about the electron-phonon coupling which can be used to test microscopic theories now in progress.[18]

ACKNOWLEDGMENTS

One of us (L.P.) wishes to thank the Solid State Division of Oak Ridge National Laboratory for its hospitality during his guest assignment while on leave from the Kernforschungszentrum Karlsruhe, Federal Republic of Germany. The technical assistance of J. L. Sellers and T. L. Collins was appreciated very much. This research was sponsored by the Division of Materials Sciences, U. S. Department of Energy, under Contract No. W-7405-eng-26 with the Union Carbide Corporation.

---

*Present address: Institut für Angewandte Kernphysik I, Kernforschungszentrum Karlsruhe, Postfach 3640, D-7500 Karlsruhe, Federal Republic of Germany.

†Present address: Keio University, Yokohama, Japan.

‡Present address: Los Alamos National Laboratory, Los Alamos, NM 87545.

[1]H. G. Smith, Aust. J. Phys. 33, 861 (1980); H. G. Smith and W. Gläser, Phys. Rev. Lett. 27, 1803 (1970); H. G. Smith, N. Wakabayashi, and M. Mostoller, in *Superconductivity in d- and f-Band Metals,* edited by D. A. Douglass (Plenum, New York, 1976), p. 223.

[2]A. Y. Rumyantsev, M. G. Zemlyanov, P. P. Parskin, N. A. Chernoplekov, U. A. Usov, and V. A. Marchenko, Fiz. Tverd. Tela (Leningrad) 19, 1715 (1977).

[3]G. Shirane and J. D. Axe, Phys. Rev. Lett. 27, 1803 (1971); J. D. Axe and G. Shirane, Phys. Rev. 30, 214 (1973); J. D. Axe and G. Shirane, Phys. Rev. B 8, 1965 (1975); G. Shirane and J. D. Axe, Phys. Rev. B 18, 3742 (1978).

[4]C. M. Varma and W. Weber, Phys. Rev. Lett. 39, 1904 (1977); C. M. Varma and W. Weber, Phys. Rev. B 19, 6142 (1979); W. Weber, in *Superconductivity in d- and f-Band Metals,* edited by H. Suhl and M. B. Maple (Academic, New York, 1980), p. 131.

[5]L. Weiss and A. Y. Rumyantsev, Phys. Status Solidi B 107, K75 (1981).

[6]J. E. Jørgensen, J. D. Axe, L. M. Corliss, and J. M. Hastings, Phys. Rev. B 25, 5856 (1982).

[7]M. Kobbelt, N. Nücker, W. Reichardt, and B. Scheerer, in *Superconductivity in d- and f-Band Metals,* edited by W. Buckel and W. Weber (Kernforschungszentrum Karlsruhe, Karlsruhe, 1982), p. 119.

[8]B. N. N. Achar and G. R. Barsch, Phys. Status Solidi B 76, 677 (1980).

[9]W. Gorzkowski, Phys. Status Solidi 3, 910 (1963).

[10]L. F. Mattheis, in Massachusetts Institute of Technology Solid State and Molecular Theory Group Quarterly Report No. 51 (unpublished).

[11]A. A. Maradudin, E. W. Montroll, G. H. Weiss, and I. P. Ipatova, in *Theory of Lattice Dynamics in the Harmonic Approximation,* 2nd ed. (Academic, New York, 1971), p. 10.

[12]S. Schicktanz, C. Kaiser, W. Weber, C. Politis, R. Flükiger, and P. Bujard, Phys. Rev. B 26, 4909 (1982).

[13]L. Pintschovius, H. G. Smith, W. Weber, W. Reichardt, N. Wakabayashi, G. Webb, Z. Fisk, Y. K. Chang, E. Aker, and C. Politis, in *Superconductivity in d- and f- Band Metals,* Ref. 7, p. 9; H. G. Smith, L. Pintschovius, N. Wakabayashi, and Y. K. Chang (unpublished).

[14]L. Pintschovius, H. G. Smith, W. Reichardt, E. Aker, and C. Politis (unpublished).

[15]S. B. Dierker, M. V. Klein, G. Webb, Z. Fisk, B. S. Chandrasehkar, J. Wernick, G. Hull, and S. Jørgensen, in *Superconductivity in d- and f-Band Metals,* Ref. 7, p. 563.

[16]B. P. Schweiss, B. Renker, E. Schneider, and W. Reichardt, in *Superconductivity in d- and f-Band Metals,* Ref. 1, p. 189.

[17]S. Schicktanz, R. Kaiser, E. Schneider, and W. Gläser, Phys. Rev. B 22, 2386 (1980).

[18]W. Weber, in *Superconductivity in d- and f-Band Metals, 1982,* Ref. 7, p. 15.